NeuroImage: Clinical 18 (2018) 60–73

Contents lists available at ScienceDirect

NeuroImage: Clinical

journal homepage: www.elsevier.com/locate/ynicl

Repeated mild blast exposure in young adult rats results in dynamic and persistent microstructural changes in the brain

Alexandra Badea[a,*,1], Alaa Kamnaksh[b,1], Robert J. Anderson[a], Evan Calabrese[a], Joseph B. Long[c], Denes V. Agoston[b,**]

[a] Center for In Vivo Microscopy, Department of Radiology, Duke University Medical Center, Durham, NC, USA
[b] Department of Anatomy, Physiology and Genetics, Uniformed Services University, Bethesda, MD, USA
[c] Blast-Induced Neurotrauma Branch, Center for Military Psychiatry and Neuroscience, Walter Reed Army Institute of Research, Silver Spring, MD, USA

ARTICLE INFO

Keywords:
White matter injury
Neurodegeneration
Traumatic brain injury

ABSTRACT

A history of mild traumatic brain injury (mTBI), particularly repeated mTBI (rmTBI), has been identified as a risk factor for late-onset neurodegenerative conditions. The mild and transient nature of early symptoms often impedes diagnosis in young adults who are disproportionately affected by mTBIs. A proportion of the affected population will incur long-term behavioral and cognitive consequences but the underlying pathomechanism is currently unknown. Diffusion tensor imaging (DTI) provides sensitive and quantitative assessment of TBI-induced structural changes, including white matter injury, and may be used to predict long-term outcome. We used DTI in an animal model of blast rmTBI (rmbTBI) to quantify blast-induced structural changes at 7 and 90 days post-injury, and their evolution between the two time points. Young adult male rats (~P65 at injury) were exposed to repeated mild blast overpressure, or anesthetized as shams, and their fixed brains were imaged using high-field (7 T) MRI. We found that whole brain volumes similarly increased in injured and sham rats from 7 to 90 days. However, we detected localized volume increases in blast-exposed animals 7 days post-injury, mainly ipsilateral to incident blast waves. Affected regions included gray matter of the frontal association, cingulate, and motor cortex, thalamus, substantia nigra, and raphe nuclei (median and dorsal), as well as white matter of the internal capsule and cerebral peduncle. Conversely, we measured volume reductions in these and other regions, including the hippocampus and cerebellum, at 90 days post-injury. DTI also detected both transient and persistent microstructural changes following injury, with some changes showing distinct ipsilateral versus contralateral side differences relative to blast impact. Early changes in fractional anisotropy (FA) were subtle, becoming more prominent at 90 days in the cerebral and inferior cerebellar peduncles, and cerebellar white matter. Widespread increases in radial diffusivity (RD) and axial diffusivity (primary eigenvalue or E1) at 7 days post-injury largely subsided by 90 days, although RD was more sensitive than E1 at detecting white matter changes. E1 effects in gray and white matter, which paralleled increases in apparent diffusion, were likely more indicative of dysregulated water homeostasis than pathologic structural changes. Importantly, we found evidence for a different developmental trajectory following rmbTBI, as indicated by significant injury x age interactions on volume. Our findings demonstrate that rmbTBI initiates dynamic pathobiological processes that may negatively alter the course of late-stage neurodevelopment and adversely affect long-term cognitive and behavioral outcomes.

1. Introduction

Mild traumatic brain injury (mTBI) occurs annually in an estimated 42 million people worldwide (Gardner and Yaffe, 2015). More commonly known as concussions, mTBIs account for ~85% of all traumatic brain injuries (TBIs) (U.S. Department of Health and Human Services, C.f.D.C.a.P., 2009). In the military, mTBIs are typically caused by the exposure to blast overpressure generated by roadside bombs or improvised explosive devices (IEDs), thus resulting in mild blast-induced TBI (mbTBI) (Ling and Ecklund, 2011). Among civilians, concussions are mainly sustained by athletes playing contact sports (e.g., football, rugby, and boxing), as well as during falls and other accidents (Voss

* Correspondence to: A. Badea, Center for In Vivo Microscopy, Department of Radiology, Box 3302, Duke University Medical Center, Durham, NC 27710, USA.
** Correspondence to: D.V. Agoston, Department of Anatomy, Physiology and Genetics, Uniformed Services University, 4301 Jones Bridge Rd, Bethesda, MD 20814, USA.
E-mail addresses: alexandra.badea@duke.edu (A. Badea), denes.agoston@usuhs.edu (D.V. Agoston).
[1] These authors contributed equally to this work.

https://doi.org/10.1016/j.nicl.2018.01.007
Received 22 September 2017; Received in revised form 8 January 2018; Accepted 9 January 2018
Available online 11 January 2018

et al., 2015). Even though the acute symptoms of a single mTBI may be mild and transient, experimental and clinical studies have found that the metabolic, biochemical, and structural changes caused by mTBIs can be cumulative and have long-term consequences (MacFarlane and Glenn, 2015; Signoretti et al., 2011). Therefore, repeated head trauma is a risk factor for late-onset behavioral, cognitive, and neurodegenerative diseases, such as chronic traumatic encephalopathy (CTE) (Gavett et al., 2011; Iverson et al., 2015; McKee et al., 2015), Parkinsonism (Tansey et al., 2007), and Alzheimer's type dementia (Daneshvar et al., 2015).

In the quest for elucidating TBI pathophysiology and its neurocognitive correIates, one of the critical gaps in knowledge is the effect of age at the time of injury. Repeated mTBI (rmTBI) most frequently affects adolescents and young adults (Prins and Giza, 2012). This is an issue of particular concern for military and civilian populations because magnetic resonance imaging (MRI) studies have shown that neurodevelopmental changes take place well into adulthood (Groeschel et al., 2010; Simmonds et al., 2014; Sowell et al., 1999). While white matter microstructure reaches adult levels during adolescence, major corticolimbic association and projection tracts mature later in adulthood, particularly in males (Asato et al., 2010; Groeschel et al., 2010; Simmonds et al., 2014). Approximately 88% of the military personnel serving in Iraq and/or Afghanistan were male, and by the end of 2010, half of all those deployed were between the age of 25 and 34, with ~322,000 under the age of 25 (Institute of, M., 2013). Although civilian and military populations are equally affected, repeated low-level blast exposure can have significant implications for young service members, the military health care system, and future force readiness.

Repeated mbTBI (rmbTBI) and rmTBIs sustained during ongoing refinement of white matter integrity can effectively alter the normal course of late-phase neurodevelopment and/or aging, and affect physiologic, cognitive, and emotional function. Diffuse white matter injury is a hallmark TBI pathology (Johnson et al., 2013; Jorge et al., 2012; Mac Donald et al., 2013; Matsushita et al., 2011; Perez et al., 2014). Furthermore, brain structures are differentially vulnerable to various injury mechanisms (e.g., Purkinje cell injury and blood-brain-barrier dysfunction in the cerebellum, diffuse axonal injury in the corpus callosum) (Meabon et al., 2016; Petrie et al., 2014) with gray-white matter interfaces, peri-vascular, and peri-ventricular regions being the most injury-prone (McKee et al., 2009, 2016). Aside from MRI modalities, particularly diffusion tensor imaging (DTI), current diagnostic tests (such as functional and behavioral assessments) are neither sensitive nor specific enough to identify individuals who have sustained a mild TBI (Goldstein, 1990; Jagoda et al., 2008; Belanger et al., 2007), thereby impeding early detection and therapeutic intervention.

DTI studies have documented persistent chronic changes in white matter following one mild TBI episode; studies performed after 3 months continue to reveal white matter pathology in areas similar to those found in the acute and sub-acute phases of mTBI (Johnson et al., 2013). Accordingly, DTI can provide a sensitive and objective means for determining the relationship of cognitive deficits to TBI, even in cases where the injury was sustained years prior to the evaluation (Kraus et al., 2007). In this study, we used DTI to assess injury-induced changes in young adult rats exposed to repeated mild blast overpressure at ~P65, the equivalent of 20 years+ in humans (Semple et al., 2013). A better understanding of the microstructual dynamics of rmbTBI pathology relative to normal, late-phase neurodevelopmental changes can help predict associated cognitive impairment or recovery, and address the issue of timely, age-relevant clinical management.

2. Materials and methods

This study consisted of two identical experiments that only differed in post-injury survival time. All rats were ordered at the same weight (and corresponding age) range, underwent the same pre-procedural treatments, and were exposed to repeated blast (or sham) at the same time relative to their arrival and acclimation. Following blast or sham exposure, rats were either terminated at 7 or 90 days post-injury (or sham). At their respective termination times, rats in the 7- and 90-day survival groups were ~2 and 5 months old, respectively.

2.1. Animals and housing conditions

Seventy-two male Sprague Dawley rats (Charles River Laboratories, Wilmington, MA) were used in this study (weight at arrival: 200–225 g; age at arrival: 49–52 days, based on date of birth supplied by the vendor). Rats were pair-housed in standard cages, with built-in filters, in a reverse 12-hour light 12-hour dark cycle with food and water ad libitum. Animals were handled according to protocols approved by the Institutional Animal Care and Use Committee at the Uniformed Services University (USU; Bethesda, MD).

2.2. Experimental groups and manipulations

All animals underwent a 5-day gentling and acclimation period. Baseline open field activity was used to create two groups, *sham* and *injured*, with no statistical differences in movement, time spent in the center/margins, or horizontal/vertical activity (Kamnaksh et al., 2012). Rat numbers were identical in the 7-day ($N = 36$; sham = 18, injured = 18) and 90-day ($N = 36$; sham = 18, injured = 18) survival groups. For the duration of the studies, rats were kept in the animal facility at USU without manipulation except for behavioral testing and blast (or sham) exposures.

On the day of the exposures, all animals (sham and injured) were transported from USU to Walter Reed Army Institute of Research (Silver Spring, MD) as described earlier (Kamnaksh et al., 2011, 2014). For the duration of the exposures, rats were kept in the preparatory area of the blast room. Rats in the sham group were anesthetized in an induction chamber with 4% isoflurane (Forane; Baxter Healthcare Corporation, Deerfield, IL) in an air mixture delivered at 2 l/min. Induction times were 6 min for the 1st exposure, and 3 min for each subsequent exposure.

2.3. Injury conditions

Rats in the injured group underwent the same procedures as their respective sham controls in addition to receiving 3 mild blasts of varying pressure to mimic the variability of field blast exposures, at 20–30 min intervals. Blast overpressure was generated using a compressed air-driven shock tube that yields a single blast overpressure wave to produce a mild injury (Kamnaksh et al., 2011, 2014; Ahmed et al., 2013). Anesthetized rats in chest protection (average weight at injury: 300 g) were placed in the shock tube holder in a transverse prone position, with the right side facing the direction of the membrane and the incident blast waves and exposed to blast in the same order. *Blast no. 1*: Mylar membrane thickness = 190.5 μm (average peak total pressure = 15.54 psi or ~107.14 kPa, positive phase duration = 9.01 ms); *blast no.2*: Mylar membrane thickness = 355.6 μm (average peak total pressure = 19.41 psi or ~133.83 kPa, positive phase duration = 10.60 ms); *blast no.3*: Mylar membrane thickness = 254 μm (average peak total pressure = 17.78 psi or ~122.59 kPa, positive phase duration = 9.22 ms). Following blast (or sham), animals were moved to an adjacent bench top for observation and then transported back to the USU animal facility.

2.4. Preparation of specimens for imaging

A subset of animals from each study (7-day group: $N = 18$; sham = 9, injured = 9; 90-day group: $N = 18$; sham = 9, injured = 9) was used for the MR/DTI analyses; all other animals were used for proteomics (in preparation). At their respective termination points, rats in the 7- and 90-day survival groups were approximately 2 and

5 months old. Rats were deeply anesthetized with isoflurane inhalant until a paw pinch produced no reflex movement, and then were transcardially perfused with a cold flush of phosphate-buffered saline (PBS) containing 10% ProHance (Gadoteridol), followed by a 4% paraformaldehyde (PFA) in PBS solution with 10% ProHance – for fixation. Perfusions were performed using a peristaltic pump (Model 323E; Watson-Marlow, Wilmington, MA). The skulls were removed and the brains post-fixed in a 4% PFA solution overnight at 4 °C and then transferred to a 1% ProHance-PFA solution until scanning.

2.5. Image acquisition and processing

Brain specimens were imaged using a 7-T magnet system (Magnex Scientific, Yarnton, Oxford, UK), equipped with 650 mT/m Resonance Research gradient coils (Resonance Research, Inc., Billerica, MA), controlled with a VnmrJ Agilent Console, using a custom-made solenoid copper coil, with 30-mm diameter.

Diffusion tensor data sets were acquired using a spin-echo pulse sequence; repetition time (TR) = 100 ms, effective echo time (TE) = 16.2 ms, and number of excitations (NEX) = 1. Diffusion preparation was achieved with a modified Stejskal-Tanner diffusion scheme (Stejskal and Tanner, 1965), which used a pair of unipolar, half-sine diffusion gradient waveforms with width $\delta = 4$ ms, separation $\Delta = 8.5$ ms, and gradient amplitude = 450 mT/m. One b0 image and six high b-value images ($b = 1500$ s/mm^2) were acquired with diffusion sensitization along six non-collinear diffusion gradient vectors: (1, 1, 0), (0, 1, 1), (1, 0, 1), (1, −1, 0), (0, 1, −1), and (−1, 0, 1). The acquisition matrix was 512 × 256 × 256 over a 40 × 20 × 20 mm field of view (FOV), and k-space was fully sampled. Images were reconstructed, resulting in isotropic spatial resolution of 78-μm. Total scan time was 12 h and 44 min per animal.

Diffusion-weighted images were processed as described in Calabrese et al. (2014), using a pipeline scripted in Perl (http://www.perl.org). Each of the six diffusion-weighted images was affinely registered to the b0 image using Advanced Normalization Tools (http://stnava.github.io/ANTs/) (Avants et al., 2011), to compensate for eddy current effects. The Diffusion Toolkit (Wang et al., 2007) (http://trackvis.org/dtk/) was used to estimate the diffusion tensor, and to produce parametric images for fractional anisotropy (FA), the primary eigenvalue or axial diffusivity (E1), radial diffusivity (RD), and apparent diffusion coefficient (ADC).

The FA, E1, RD, and ADC images were processed using a voxel-based analysis pipeline scripted in Perl. Briefly, all images were skull stripped (Badea et al., 2007), rigidly aligned to an atlas, then a sequence of affine and diffeomorphic registrations was used to create a minimum deformation template (MDT) based on the sham (control) animals; all injured animals were then registered to the MDT. We used a multiresolution, 4-level registration scheme, with shrink factors 6 × 4 × 2 × 1 and 4 × 2 × 1 × 0 smoothing. For the rigid and affine transforms, we used the Mattes mutual information metric, with 32 bins, a gradient step size of 0.1, 3000 iterations for the first two levels only, and a convergence window of 20, threshold of 10^{-7}. For the diffeomorphic transforms, we used a cross-correlation metric, with a kernel radius of 4, a SyN gradient step size of 0.4, update velocity field regularization 3, and total deformation regularization 1, 500 × 500 × 500 × 50 iterations, and a convergence window of 15, threshold of 10^{-7}.

After image registration, voxel-wise comparisons of diffusion tensor parameters were carried out using statistical parametric mapping (SPM) (Friston et al., 1994). To assess volume changes, we used a simple version of tensor-based morphometry, where the volume changes from each individual were encoded to the MDT by the Jacobian determinants of deformation fields (Friston et al., 2006). To symmetrize the distributions of the Jacobians relative to zero, with similar probabilities for expansion and contraction, these were log transformed (Leow et al., 2006). Only local volumes were used for voxel-based statistics in the space of the MDT, and these were based on the diffeomorphic components alone. The diffusion tensor parametric images were mapped into the MDT space using a combined set of rigid, affine and diffeomorphic transforms, so that FA, E1, RD, and ADC could be statistically compared.

Regional measures for volume and DTI parameters were obtained after mapping a DTI-based reference atlas of the rat brain (Johnson et al., 2012), labeled with 27 anatomical regions (Calabrese et al., 2013), to the minimum deformation template (MDT). This effectively labeled the MDT with 27 atlas regions. Using the inverse transforms, mapping each individual brain to the MDT to propagate MDT labels onto each individual brain, labels were then used to quantify regional volumes and DTI parameters for each individual brain.

2.6. Statistical analysis

We analyzed differences between sham and injured groups in volume, FA, E1, RD, and ADC. All image data were spatially smoothed using a 3 × 3 × 3 voxel kernel, to help with the normality of the voxel value distribution. A cluster size threshold was set to 200 voxels to exclude spurious results from the analysis. Avizo (FEI, Burlington, MA) was used to visualize the results, presented as t maps, thresholded at the 0.05 significance level (corrected in the main manuscript figures, uncorrected in Supplementary figures), and overlaid on the minimum deformation FA template. To correct for multiple comparisons, we used a cluster-based false discovery rate (FDR) with a cluster defining threshold of 0.05. Regional-based statistics were performed in MATLAB (MathWorks, Natick, MA) using a two-way analysis of variance (ANOVA) followed by post-hoc Dunn-Sidak corrections for familywise Type I error rates at the 0.05 level. Numeric values for all ROI-based measures and related ANOVA output are provided in Supplementary tables 1–5. Select data on regional measures are presented as figures using box plots, which show the median (red line), quartiles (blue box: 25–75% of data), and range (whiskers); outliers (values above or below 1.5× the interquartile range) are shown as + signs.

3. Results

DTI data from sham and injured brains were compared between the various experimental groups to determine: (1) the short-term effect of repeated exposure to mild blast overpressure on brain structures: comparing injured to control rats 7 days after 3× blast (or sham) exposure; (2) the long-term effect of repeated exposure to mild blast overpressure on brain structures: comparing injured to control rats 90 days after 3× blast (or sham) exposure; (3) the effect of normal aging on brain volume and microstructural integrity: comparing sham rats at the age of 2 months to sham rats at the age of 5 months, corresponding to the 7- vs. 90-day survival time points; (4) the effect of injury on age-related changes: between the age of 2 months (corresponding to 7-day survival) and 5 months (corresponding to 90-day survival).

3.1. Volumetric measures

3.1.1. Injury effects at 7 and 90 days post-exposure

We examined brain volume differences between injured and control rats at two post-injury (or sham) time points. At 7 days, local gray matter volume increases were noted in injured rats compared to age-matched controls in the olfactory and frontal association cortex, striatum, cingulate and motor cortex, thalamus, substantia nigra, tectum (superior colliculus), raphe nuclei (median and dorsal), and the isthmic reticular nucleus (Fig. 1A). Among white matter tracts, the internal capsule and cerebral peduncle appeared unilaterally enlarged. At 90 days post-injury we noted volume reductions in the cingulate cortex, caudate putamen, and globus pallidus, as well as the thalamus (covering the superior thalamic radiation, medial lemniscus), hippocampus

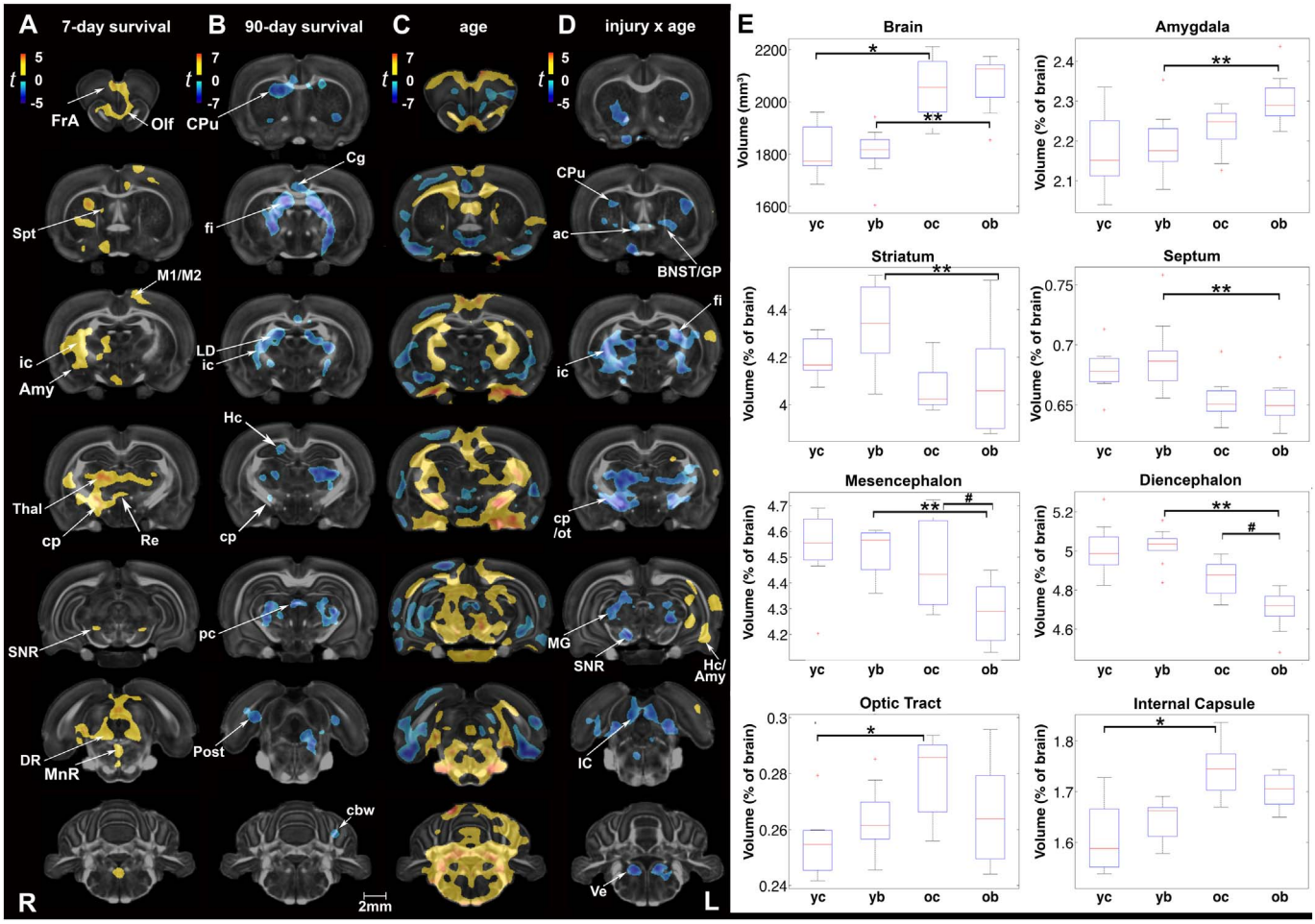

Fig. 1. Short- and long-term changes in volume between injured and sham rats. (A) At 7 days post-injury, local gray matter volume increases were noted in injured rats in the olfactory (Olf) and frontal association (FrA) cortex, striatum, cingulate and motor (M1/M2) cortex, thalamus (Thal), substantia nigra (SNR, reticular part), tectum (superior colliculus), median and dorsal raphe nuclei (MnR and DR, respectively), and the isthmic reticular nucleus (Re). Among white matter tracts, the internal capsule (ic) and cerebral peduncle (cp) appeared unilaterally enlarged. (B) At 90 days post-injury, we noted volume reductions in the cingulate cortex (Cg), caudate putamen (CPu), and globus pallidus, as well as the thalamus, hippocampus (Hc), and postsubiculum (Post). White matter tracts with reduced volume included the corpus callosum, fimbria (fi), internal capsule (ic), cerebral peduncle (cp), posterior commissure (pc), and cerebellar white matter (cbw). (C) Age-related changes in control rats (2-month vs. 5-month old) were predominantly marked by volume increases, particularly in the hindbrain, with variable reductions in the gray matter volume of piriform, hypothalamic, and hippocampal regions. (D) Interactions on volume were predominantly negative in the CPu, globus pallidus (GP), bed nucleus of the stria terminalis (BNST), thalamus, SNR, and tectum (superior and inferior colliculus). A negative interaction was also observed for white matter tracts including the anterior commissure (ac), fi, ic, cp, and optic tract (ot). In contrast, areas of the hippocampus (Hc) and amygdala (Amy) showed positive interactions (unilateral). Voxel-wise data are presented as *t* maps, cluster-corrected for multiple comparisons, and thresholded at the 0.05 significance level; R = right (ipsilateral hemisphere), L = left (contralateral hemisphere); scalebar = 2 mm. (E) Total brain volume (mm^3) and normalized regional volumes (% of brain) at 7 and 90 days post-injury (or sham). ROI data are presented as box plots where red line = median, box = quartiles, whiskers = range, + = outliers; significant group differences ($p < .05$) are denoted as follows: * age-related changes in control rats; ** age-related changes in injured rats; # injury-related differences between age-matched groups. Key: IC, inferior colliculus; LD, laterodorsal thalamic nucleus; MG, medial geniculate nucleus; Spt, septum; Ve, vestibular nuclei; yc, young control; yb, young blast; oc, old control; ob, old blast.

and postsubiculum, and cerebellum (Fig. 1B). White matter tracts with reduced volume included the corpus callosum, fimbria, internal capsule, cerebral peduncle, posterior commissure, and cerebellar white matter.

Uncorrected statistical maps also showed volume reductions in the hippocampus at 7 days post-injury, and in the inferior colliculus (starting at 7 days and becoming more prominent at 90 days). In contrast, local volume increases were noted in the piriform cortex and amygdala, the latter progressing from 7 to 90 days after injury (Suppl. Fig 1).

Using atlas-based segmentation, we calculated total brain volume (mm^3) and 28 regional volumes (as a percentage of total brain volume) at the two survival times. A two-way ANOVA of the normalized region of interest (ROI) volumes revealed significant main effects of injury, age, and injury × age interactions (Suppl. Table 1A). At 7 days post-injury, we did not observe significant group differences in total or regional brain volumes; only a trend was observed in the striatum, ~3% larger in injured animals ($p = .07$, $t = 1.95$). Consistent with the volume changes at 7 days, we did not detect global brain size differences between sham and injured animals at 90 days post-exposure. However, small but significant volume reductions were noted in injured rats relative to controls in the normalized volumes of the mesencephalon (4% smaller, $p = .03$) and diencephalon (3% smaller, $p = .02$) (Fig. 1E; Suppl. Table 1B). Conversely, volume was increased in the cervical portion of the spinal cord of injured rats at 90 days post-exposure (7% difference, $p = .03$), although measurement accuracy in this region is reduced since the measured segment is only defined as a small portion of the spinal cord in our brain atlas. Furthermore, it is difficult to rule out experimental bias in sectioning the cord during the preparation of specimens.

3.1.2. *Age effects and interactions with injury*

Voxel-based statistical maps revealed age-related changes in several white and gray matter regions. Age effects in control animals were

predominantly marked by increases in volume, covering extensive areas of the hindbrain (Fig. 1C). Compensatory reductions in volume were also noted in the piriform, hypothalamic, and hippocampal areas of control brains. ROI analysis revealed that total brain volumes were still increasing between the ages of 2 and 5 months in both sham ($1814 \pm 37\,mm^3$ to $2054 \pm 34\,mm^3$; 13% difference, $p < .001$) and injured rats ($1806 \pm 34\,mm^3$ to $2076 \pm 34\,mm^3$; 15% difference, $p < .001$) (Fig. 1E).

Although age-related increases in total volume were similar in the two groups, we found significant injury x age interactions on volume (Fig. 1D). Interactions were predominantly negative and included olfactory areas, the striatum, globus pallidus, bed nucleus of the stria terminalis, thalamus, substantia nigra, tectum (superior and inferior colliculus), as well as vestibular nuclei. A negative interaction was also observed for white matter tracts including the anterior commissure, fimbria, internal capsule, cerebral peduncle, and optic tract. In contrast, areas of the hippocampus and amygdala (unilateral) showed positive interactions. Of note, these clusters of positive interactions were observed on the contralateral side of blast impact. At a regional level, injury × age interactions were significant for the normalized volumes of the diencephalon ($F_{1,31} = 5.85$, $p = .02$), hippocampus ($F_{1,31} = 5.2$, $p = .03$), bed nucleus of the stria terminalis ($F_{1,31} = 5.75$, $p = .02$), and spinal cord ($F_{1,31} = 5.13$, $p = .03$). Among white matter ROIs, the interactions were significant for the internal capsule ($F_{1,31} = 4.67$, $p = .04$) and optic pathways ($F_{1,31} = 4.72$, $p = .04$).

3.2. Fractional anisotropy (FA)

3.2.1. Injury effects at 7 and 90 days post-exposure

In voxel-based analysis, no significant group differences in FA were detected at 7 days after correcting for multiple comparisons. At 90 days, FA was increased in injured rats relative to shams in the gray matter of olfactory regions, anterior hypothalamus, the centromedial thalamic nucleus, hippocampus (unilateral), periaqueductal gray, cerebellum, and gigantocellular reticular nucleus of the brainstem. White matter tracts marked by FA increases included the cerebral peduncles, inferior cerebellar peduncle, spinal trigeminal tract, and cerebellar white matter (Fig. 2A).

Uncorrected statistics suggest that at 7 days post-injury FA decreased in white matter areas of the corpus callosum, optic chiasm, and cerebral peduncle, and conversely increased in the internal capsule, external capsule (unilateral), and cerebellar white matter. Gray matter regions characterized by FA increases included the motor (M1/M2), cingulate (A30), septum, and brainstem reticular (e.g., gigantocellular) areas (Suppl. Fig. 2A). By 90 days, FA increases appeared to be more symmetric for the striatum, hippocampus, entorhinal and visual cortices (Suppl. Fig. 2B).

At the ROI level, there were no significant injury effects on FA, neither at 7 days nor at 90 days post-exposure, except in the axial hindbrain ($F_{1,31} = 5.85$, $p = .02$) (Suppl. Table 2A). FA was ~9% higher in the axial hindbrain of injured rats relative to sham rats at 90 days.

3.2.2. Age effects and interactions with injury

Age-related changes in white and gray matter microstructure were marked by FA increases between 2 and 5 months in sham animals (Fig. 2B). Two-way ANOVAs revealed significant main effects of age on FA in several white and gray matter ROIs (Suppl. Table 2A). Post-hoc tests revealed significant age-related changes in the same ROIs for both control and injured rats, although the extent of FA changes between 2 and 5 months was greater in injured rats and included the hippocampal formation (Suppl. Table 2B).

The interaction effect did not survive multiple comparison corrections. However, in uncorrected voxel-based statistical maps, we observed largely positive injury x age interactions on FA in both white and gray matter regions (Suppl. Fig. 2C). White matter areas included the lateral olfactory tract, optic chiasm, corpus callosum, hippocampus, cerebellar peduncle, and cerebellar white matter. Gray matter areas included the olfactory, cingulate, primary somatosensory and insular cortices, as well as the hypothalamus, hippocampus, amygdala, regions of the brainstem, and cerebellum. At a regional level, significant injury x age interactions on FA were limited to the pituitary ($F_{1,31} = 4.69$, $p = .04$) (Suppl. Table 2A).

3.3. Axial diffusivity (E1)

3.3.1. Injury effects at 7 and 90 days post-exposure

Voxel-based analysis indicated extensive increases in E1 at 7 days post-injury (Fig. 3A). Gray matter regions with increased E1 included the cingulate, sensory, motor and visual cortices. White matter areas with increased E1 were found in the corpus callosum, cingulum, internal capsule, stria medularis, superior thalamic radiation/medial lemniscus, and fimbria, as well as the medial longitudinal fasciculus, all cerebellar peduncles, and cerebellar white matter. By 90 days, E1 increases had largely subsided; group differences did not survive multiple comparison correction. However, in uncorrected statistics E1 was still larger at 90 days in the cerebral peduncle, inferior cerebellar peduncle, and small clusters in the corpus callosum and spinocerebellar tract (Suppl. Fig. 3B).

Regional injury-related differences in E1 were significant in the axial hindbrain and the spinal cord (Suppl. Table 3A). Mean E1 values were highest at 7 days post-injury in injured animals in 17 of the 27 ROIs. Importantly, the amygdala and cerebellum were among the regions with increased E1 at 90 days post-injury.

3.3.2. Age effects and interactions with injury

We did not detect significant age-related changes in E1 after correcting for multiple comparisons. Uncorrected statistics showed higher E1 in the gray matter of young rats (7-day survival) relative to older rats (90-day survival), with the reverse in white matter structures like the cerebral peduncle, inferior cerebellar peduncle, and spinal trigeminal tract (data not shown). A negative injury × age interaction effect was largely confined to the cerebellum in uncorrected statistics only. Small clusters were also identified in the corpus callosum, amygdala, inferior colliculus, and entorhinal cortex (Suppl. Fig. 3C).

At the ROI level, age effects on E1 were significant for the axial hindbrain, amygdala, and optic pathways, such that E1 values were higher in 5-month-old controls relative to younger counterparts (Suppl. Table 3A). After correcting for multiple comparisons, significant changes in E1 were limited to the optic pathways ($F_{1,31} = 13.44$, $p = .04$) and amygdala ($F_{1,31} = 12.11$, $p = .05$) (Fig. 3B; Suppl. Table 3B).

3.4. Radial diffusivity (RD)

3.4.1. Injury effects at 7 and 90 days post-exposure

Voxel-based analysis revealed RD increases in injured rats relative to age-matched controls in the primary motor, sensory, visual, and cingulate cortices (Fig. 4A). The hippocampus (unilateral), septum, superior colliculus, periaqueductal gray, and cerebellar gray matter also had increased RD. White matter tracts with increased RD included the corpus callosum and cingulum, anterior commissure, internal capsule (unilateral), cerebral as well as the inferior cerebellar peduncle, spinal trigeminal tract, pyramids, as well as cerebellar white matter. At 90 days post-injury, RD increases had normalized and differences between injured and sham rats were insignificant (not shown).

ROI analysis indicated that at 7 days post-injury RD was ~15% higher in injured animals relative to controls in the corpus callosum ($F_{1,31} = 4.52$, $p = .049$) (Fig. 4B). In fact, mean RD values were highest in injured animals at 7 days in all ROIs except the pituitary, ventricles, optic pathways, pineal gland, and spinal cord (Suppl. Table 4A). At 90 days post-injury, there were no significant group differences in RD.

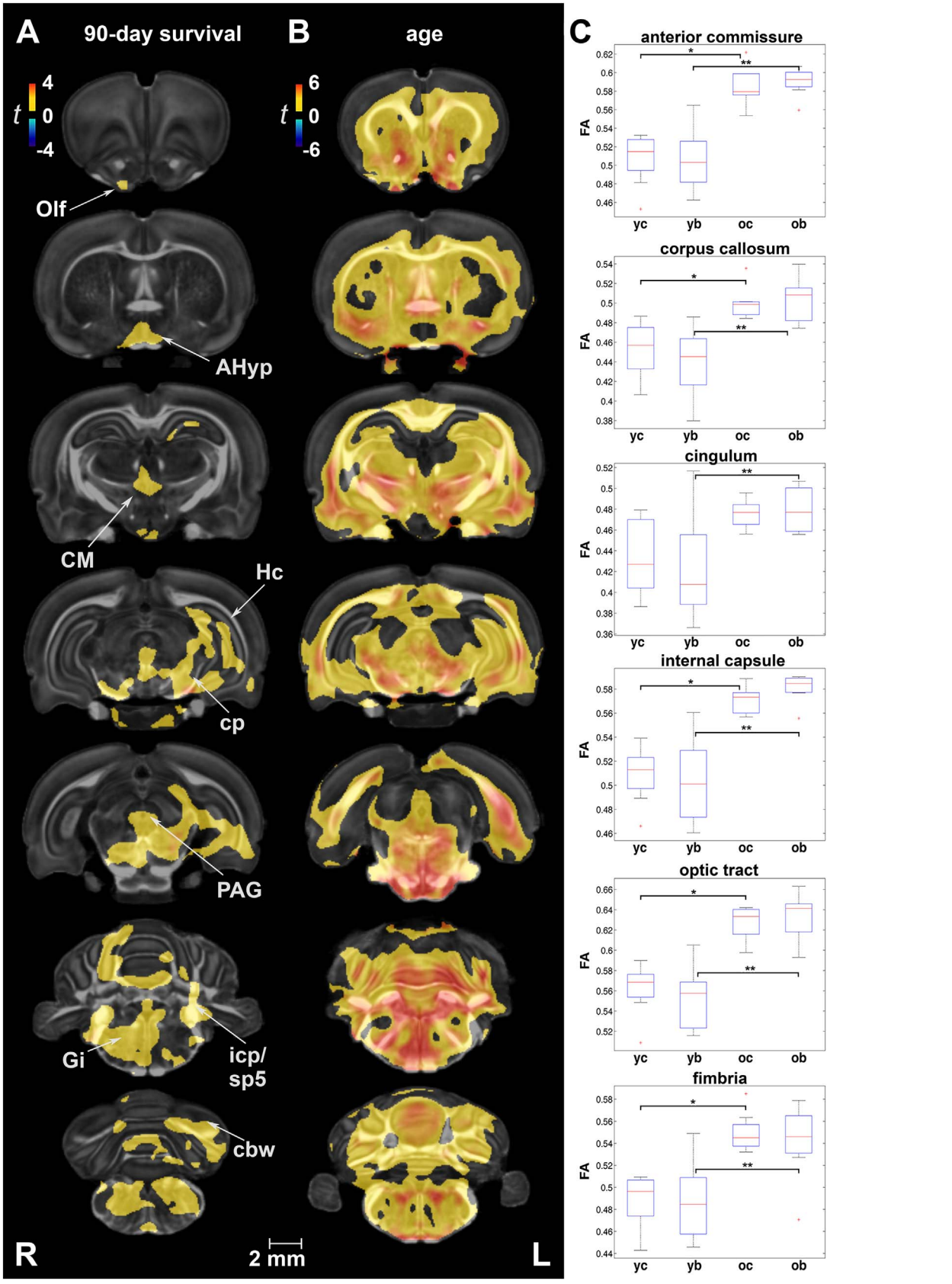

(caption on next page)

Fig. 2. Fractional anisotropy (FA) was sensitive at detecting long-term changes in gray and white matter following repeated mild blast exposure as well as age effects. (A) At 90 days post-injury, FA was increased in injured rats relative to age-matched controls in gray matter of olfactory regions (Olf), anterior hypothalamus (AHyp), the centromedial thalamic nucleus (CM), hippocampus (Hc), periaqueductal gray (PAG), cerebellum, and gigantocellular reticular nucleus (Gi). White matter tracts marked by FA increases included the cerebral peduncles (cp), inferior cerebellar peduncle (icp), spinal trigeminal tract (sp5), and cerebellar white matter (cbw). (B) Age-related changes in FA, consistent with normal neurodevelopment, were extensive in white and gray matter. Voxel-wise data are presented as *t* maps, cluster-corrected for multiple comparisons, and thresholded at the 0.05 significance level; R = right (ipsilateral hemisphere), L = left (contralateral hemisphere); scalebar = 2 mm. (C) FA (unitless) was significantly higher at 90 days post-injury (or sham) for white matter regions of interest. ROI data are presented as box plots where red line = median, box = quartiles, whiskers = range, + = outliers; significant group differences ($p < .05$) are denoted as follows: * age-related changes in control rats; ** age-related changes in injured rats. Key: yc, young control; yb, young blast; oc, old control; ob, old blast.

3.4.2. Age effects and interactions with injury

While we did not detect a significant difference in RD with age following multiple comparison correction of voxel-based analysis, we noted that age-related changes in RD were marked by decreases in uncorrected statistics (Suppl. Fig. 4B). A negative injury × age interaction was noted for RD only before multiple comparison correction in areas of the corpus callosum, 5th/trigeminal nerve, and medial longitudinal fasciculus. The same pattern was observed for gray matter structures like the olfactory, cingulate, and visual (V2) cortices, as well as the temporal association and ectorhinal cortices, and cerebellum (Suppl. Fig. 4C).

At a regional level, we detected significant age-related RD decreases in control rats in the anterior commissure ($F_{1,31} = 27.71$, $p = .04$). RD was also significantly lower in the anterior commissure ($t = -4.14$, $p < .001$), corpus callosum ($t = -4.19$, $p < .001$), cingulum ($t = -3.89$, $p = .001$), and internal capsule ($t = -2.90$, $p = .01$) of 5-month old injured rats than in their younger counterparts (Fig. 4B). Importantly, RD changes in these white matter ROIs remained significant after correcting for familywise error and included additional gray matter regions in injured animals (Suppl. Table 4B). Age-related reductions in RD were observed in the substantia nigra ($F_{1,31} = 9.81$, $p = .02$), diencephalon ($F_{1,31} = 10.13$, $p = .02$), pallidum ($F_{1,31} = 10.73$, $p = .02$), and nucleus accumbens ($F_{1,31} = 10.03$, $p = .05$).

3.5. Apparent diffusion coefficient (ADC)

3.5.1. Injury effects at 7 and 90 days post-exposure

The pattern of ADC changes paralleled E1 increases, which were significant and widespread at 7 but not at 90 days post-exposure (Fig. 5). Areas characterized by early injury-induced ADC differences included the anterior commissure, corpus callosum and cingulum, internal capsule, cerebellar peduncles (all three) and cerebellar white matter, as well as the spinocerebellar and spinal trigeminal tracts. Gray matter also has increased ADC in areas of the motor, sensory, visual, and cingulate cortices, periaqueductal gray, tectum, and extensive areas of the cerebellum. Uncorrected statistics at 7 and 90 days post-injury, respectively, are available in Suppl. Fig. 5A and B. At 90 days post-injury, small regions of increased ADC were present only in the corpus callosum, lateral olfactory and optic tract, the inferior cerebellar peduncle, and spinocerebellar tract of injured rats.

Mean ADC values were highest in injured rats at 7 days post-injury for the majority of ROIs (Suppl. Table 5A). However, there were no significant differences in ADC between injured and sham rats at either termination time point.

3.5.2. Age effects and interactions with injury

In voxel-based statistical maps, there were no significant effects for age or injury x age interactions on ADC. At a regional level, two-way ANOVAs yielded a main effect for age in several ROIs (Suppl. Table 5A). Post-hoc comparisons revealed significantly higher ADC values in the anterior commissure ($F_{1,31} = 8.81$, $p = .05$), cingulum ($F_{1,31} = 7.47$, $p = .03$), and corpus callosum ($F_{1,31} = 11.34$, $p = 5.7 \times 10^{-3}$) of injured rats at 7 days than at 90 days post-exposure (Suppl. Table 5B).

4. Discussion

In our study of young adult rats exposed to repetitive mild blast, we have used high-resolution DTI to examine the effects of injury at an early and late timepoint toward a better understanding of rmbTBI pathology and its evolution. We found significant injury-induced changes in volume and diffusion tensor parameters in the subacute and chronic phase of the injury, as well as differing temporal changes in these measures, thus demonstrating the sensitivity and diagnostic utility of DTI in rmbTBI. Volume changes indicated significant injury x age interactions—particularly in the caudate putamen/striatum, thalamus/diencephalon, bed nucleus of the stria terminalis (BNST), and internal capsule—while DTI parameters were sensitive at capturing age and injury-related microstructural changes, highlighting the vulnerability of the corpus callosum, axial hindbrain, and cerebellum to repeated blast exposure. The most important aspect of our findings is the dynamic nature of these changes, as they continued to evolve over time, suggesting a complex interplay of neuroplasticity and rmbTBI pathology.

The innate malleability of the developing brain confers numerous advantages against injury and disease, including increased resilience and quicker recovery. But neuroplasticity can also change the developmental trajectory of the brain and have far-reaching functional implications following traumatic incidents (Emery et al., 2003; Gritti et al., 2002; Lewis, 2004; Selemon, 2013). While increased brain metabolism and synaptic activity have been found to promote recovery after focal injury (Kolb et al., 1998), it is not well-understood how these features impact the deleterious effects of more diffuse injuries (e.g., concussion or mbTBI) that are compounded by the selective vulnerability of brain structures (Meabon et al., 2016; Petrie et al., 2014). Furthermore, the heterogeneity of primary blast injury and multitude of secondary injury mechanisms result in various pathological changes (Cernak and Noble-Haeusslein, 2010), including neuroinflammation, as indicated by gliosis and microglial infiltration (Bauman et al., 2009; Long et al., 2009), changes in dendritic morphology (Zuckerman et al., 2017), and progressive white matter pathology (Winston et al., 2016). To help fill the current knowledge gap concerning the effect of repeated mild head injury on the temporal trajectory of late-phase neurodevelopment, we used translational MR imaging methods to assess injury-induced changes in volume and diffusion tensor parameters relative to normal aging.

4.1. Volumetric changes following repeated mild blast exposure suggest an altered maturational trajectory

MRI studies of developing human brains have consistently observed increases in total brain volume along with regionally variable reductions in gray matter volume (Groeschel et al., 2010; Sowell et al., 2001, 2002). Cross-sectional imaging studies have found age-related reductions in the volume of cortical gray matter regions, as well as deep gray matter structures including the pallidum, amygdala, and hippocampus (Giorgio et al., 2010; Scahill et al., 2003). These reductions typically occur in the context of increasing white matter volume and myelination in peripheral regions of the cortex (Asato et al., 2010; Sowell et al., 1999), beginning in early adulthood and continuing throughout adulthood in an approximately linear manner (Giorgio et al., 2010). Longitudinal MRI studies of rat brains have shown that neurodevelopmental changes are most prominent during the first 2–3 months of life

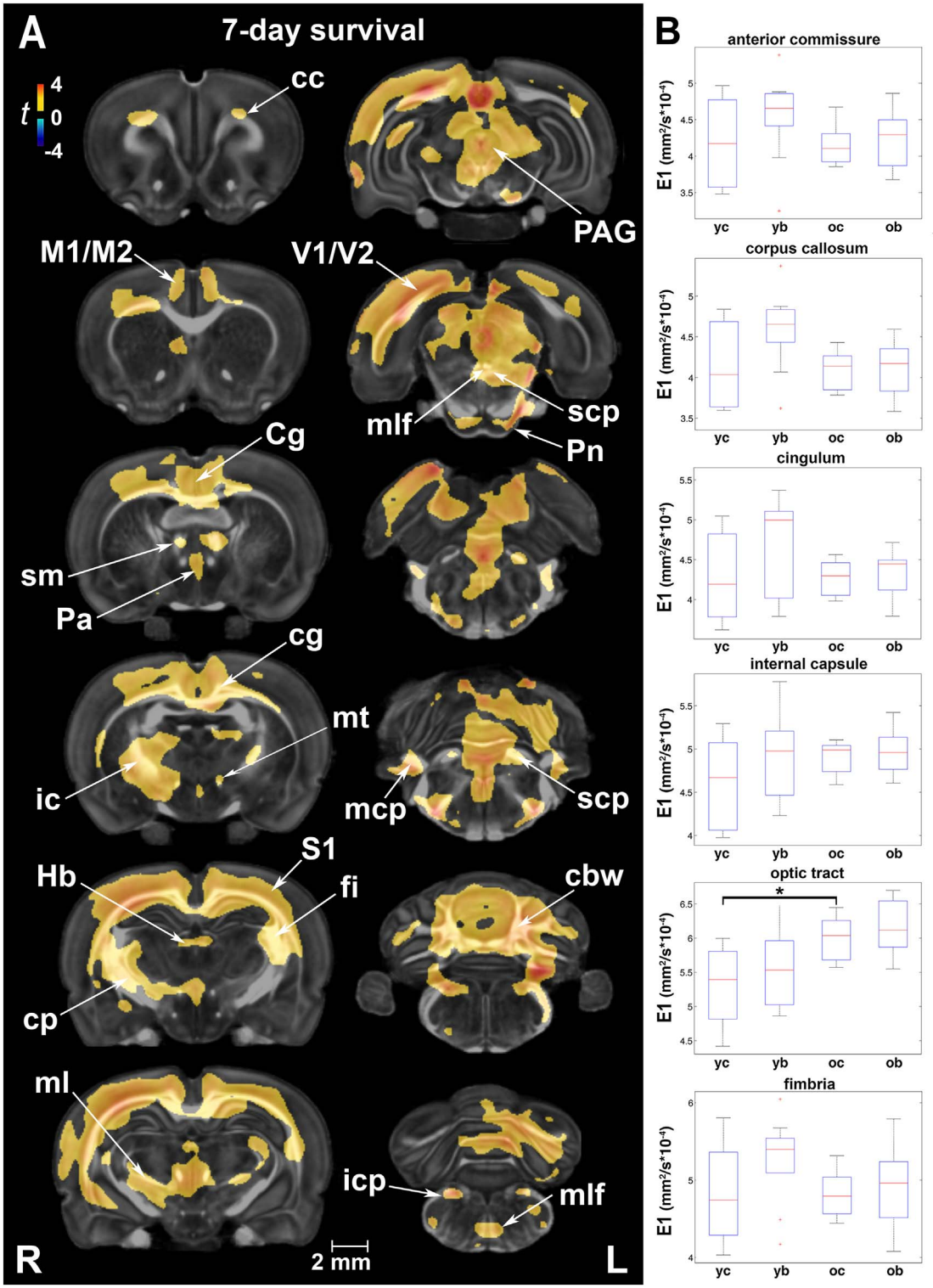

Fig. 3. Early changes in axial diffusivity (E1) after injury were extensive, albeit transient. (A) E1 differences between injured and sham rats covered a large number of gray and white matter areas. Gray matter regions with increased E1 included the cingulate (Cg), sensory (S1), motor (M1/M2), and visual (V1/V2) cortices. White matter areas with increased E1 were found in the corpus callosum (cc), cingulum (cg), internal capsule (ic), stria medularis (sm), superior thalamic radiation/medial lemniscus (ml), and fimbria (fi), as well as the medial longitudinal fasciculus (mlf), all cerebellar peduncles (scp, mcp, and icp), and cerebellar white matter (cbw). Voxel-wise data are presented as *t* maps, cluster-corrected for multiple comparisons, and thresholded at the 0.05 significance level; R = right (ipsilateral hemisphere), L = left (contralateral hemisphere); scalebar = 2 mm. (B) On a regional level, the only significant finding was an increase in E1 ($mm^2/s \times 10^{-4}$) with normal maturation for the optic tract ($p = .04$). ROI data are presented as box plots where red line = median, box = quartiles, whiskers = range, + = outliers. Key: cp, cerebral peduncle; Hb, habenular nuclei; icp, inferior cerebellar peduncle; mcp, middle cerebellar peduncle; mt, mammillothalamic tract; Pa, paraventricular hypothalamic nucleus; PAG, periaqueductal gray; Pn, pontine nuclei; S1, primary somatosensory cortex; scp, superior cerebellar peduncle; yc, young control; yb, young blast; oc, old control; ob, old blast.

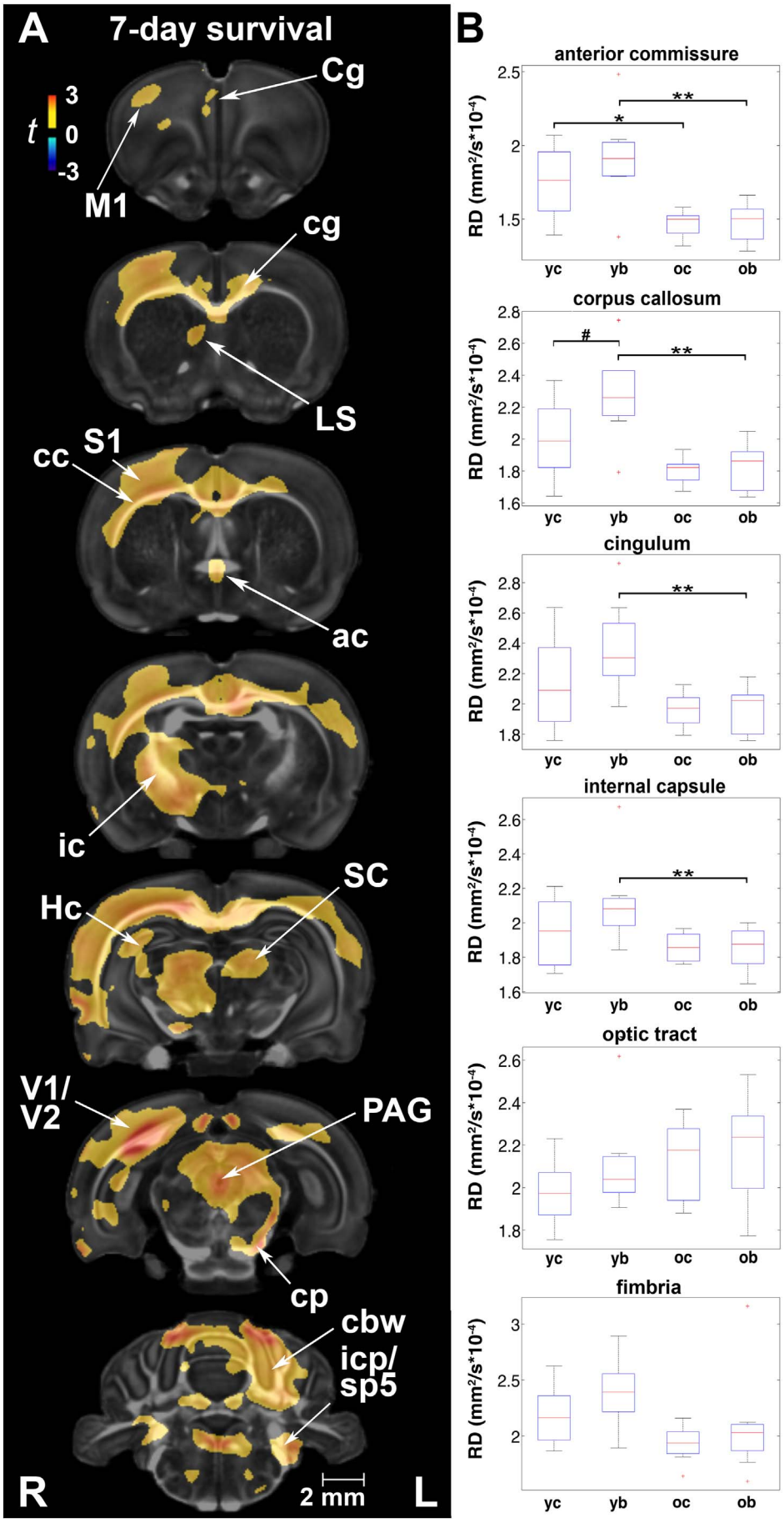

Fig. 4. Radial diffusivity (RD) was most sensitive at detecting changes in white matter properties following rmbTBI. (A) The most conspicuous difference in RD between injured and sham animals was at 7 days post-exposure in the ipsilateral motor (M1), sensory (S1), visual (V1/V2), and cingulate (Cg) cortex, as well as the hippocampus (Hc), lateral septal nucleus (LS), periaqueductal gray (PAG), and cerebellar gray matter. White matter tracts with increased RD included the corpus callosum (cc), cingulum (cg), anterior commissure (ac), internal capsule (ic), pyramids, and cerebellar white matter (cbw). Voxel-wise data are presented as *t* maps, cluster-corrected for multiple comparisons, and thresholded at the 0.05 significance level; R = right (ipsilateral hemisphere), L = left (contralateral hemisphere); scalebar = 2 mm. (B) Blast-induced increases in RD ($mm^2/s \times 10^{-4}$) were significant in the corpus callosum at 7 days post-injury. ROI data are presented as box plots where red line = median, box = quartiles, whiskers = range, + = outliers; significant group differences ($p < .05$) are denoted as follows: * age-related changes in control rats; ** age-related changes in injured rats; # injury-related differences between age-matched groups. Key: cp, cerebral peduncle; cg, cingulum; icp, inferior cerebellar peduncle; SC, superior colliculus; sp5, spinal trigeminal tract; yc, young control; yb, young blast; oc, old control; ob, old blast.

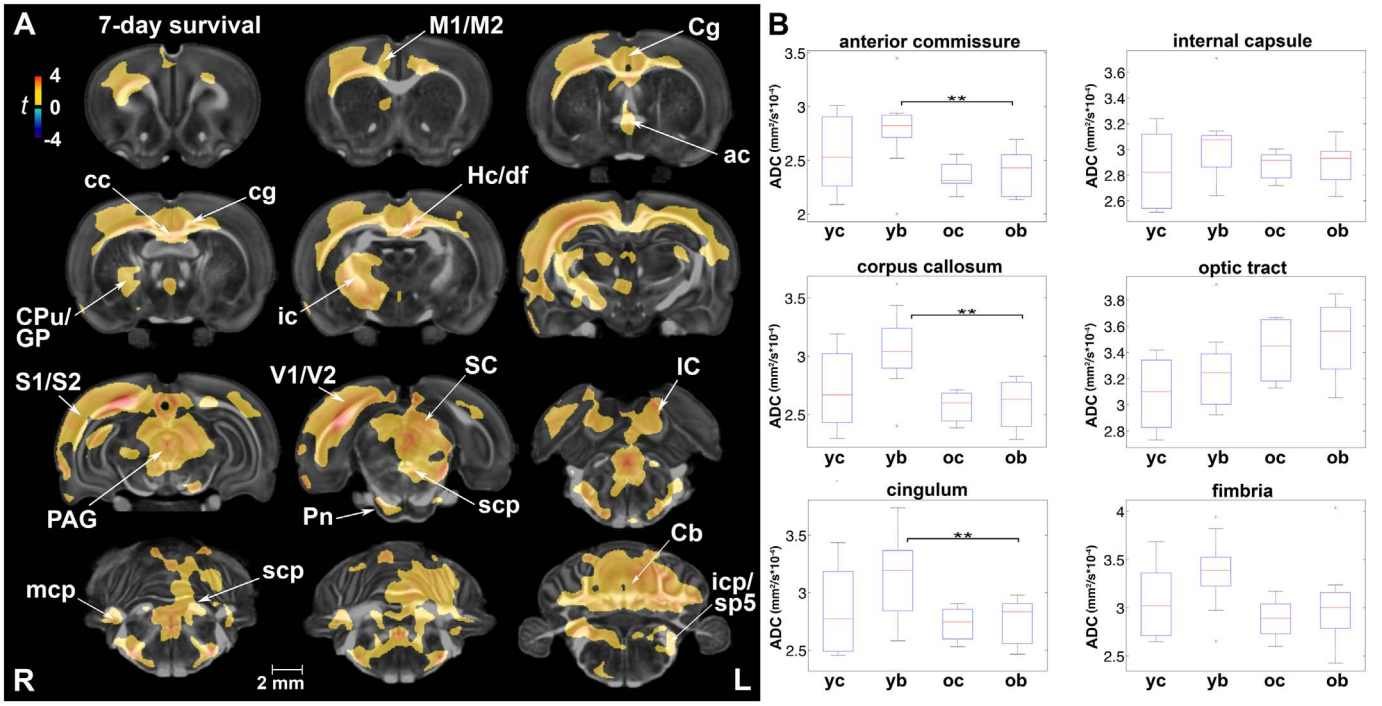

Fig. 5. Apparent diffusion coefficient (ADC) paralleled changes in axial diffusivity following repeated mild blast exposure. (A) White matter areas characterized by early injury-induced ADC differences included the corpus callosum (cc), cingulum (cg), anterior commissure (ac), internal capsule (ic), cerebellar peduncles (all three; scp, mcp, and icp), and cerebellar white matter. ADC was similarly increased at 7 days post-injury in gray matter areas of the motor (M1/M2), sensory (S1/S2), visual (V1/V2), and cingulate (Cg) cortex, periaqueductal gray (PAG), tectum, and extensive areas of the cerebellum (Cb). Voxel-wise data are presented as *t* maps, cluster-corrected for multiple comparisons, and thresholded at the 0.05 significance level; R = right (ipsilateral hemisphere), L = left (contralateral hemisphere); scalebar = 2 mm. (B) Mean ADC values ($mm^2/s \times 10^{-4}$) were highest in injured rats at 7 days post-injury, although there were no significant differences between injured and control rats at the regional level. ROI data are presented as box plots where red line = median, box = quartiles, whiskers = range, + = outliers; significant group differences ($p < .05$) are denoted as follows: ** age-related changes in injured rats. Key: CPu, caudate putamen; GP, globus pallidus; Hc/df, hippocampus/dorsal fornix; IC, inferior colliculus; icp, inferior cerebellar peduncle; mcp, middle cerebellar peduncle; Pn, pontine nuclei; sc, spinocerebellar tract; SC, superior colliculus; scp, superior cerebellar peduncle; sp5, spinal trigeminal tract; yc, young control; yb, young blast; oc, old control; ob, old blast.

(Calabrese et al., 2013; Mengler et al., 2014; Semple et al., 2013; Sumiyoshi et al., 2017). After this time, cortical myelination accretion is observed using histological analysis for at least six months (Mengler et al., 2014).

Our earlier quantitative morphometric analysis of rat brain development revealed remarkable spatiotemporal heterogeneity in the volumes of cortical, subcortical, and white matter-rich structures (Calabrese et al., 2013). While the volumes of structures like the isocortex and hippocampus appear to plateau around P40, structures rich in white matter (e.g., hindbrain) exhibit nearly linear growth during late-phase development. In our current study, we measured increases in whole brain volume between the ages of 2 months (corresponding to 7-day survival groups) and 5 months (corresponding to 90-day survival groups) in both control and injured rats, with no statistically significant differences in total volume between the two groups. However, regional volume changes in each group provide evidence for differing developmental/aging trajectories.

Regional brain volumes of control rats generally increased except in the entorhinal cortex/hippocampal formation, preoptic/hypothalamic regions, olfactory tubercule, and small areas of the isocortex. Compensatory volume decreases in control rats are likely related to tissue reorganization processes that include increased myelination and cell density, which result in less extracellular space for water (Mengler et al., 2014). Compared to their age-matched controls, long-term regional volume changes in injured rats point to a different growth trajectory following rmbTBI. Initially, local volumes increased at 7 days post-injury, a hallmark early response due to disruptions in ion and water homeostasis following TBI (Ling et al., 2012). Although injury-induced volumetric increases were bilateral, they were more pronounced ipsilateral to incident blast waves. This observation is consistent with previous findings indicating greater damage in the hemisphere facing the shock tube (Long et al., 2009). In the late phase of the injury, blast-exposed rats showed local atrophy in the caudate putamen, cingulate cortex, thalamus, hippocampal formation (post subiculum), and cerebellum. Affected white matter tracts included the corpus callosum, cingulate and motor cortex, internal capsule, and fimbria. Importantly, we found significant injury × age interactions on volume in many of these regions.

Negative interactions on the local volumes of gray and white matter structures suggest persistent injury-induced changes and/or impaired development following repetitive blast injury. Interactions in structures involved with vestibular, dopaminergic nigrostriatal pathway (caudate putamen, substantia nigra), and associated movement pathways point to circuits with selective vulnerability in movement disorders and/or Parkinsonism (Acosta et al., 2015; Huang et al., 2017). Furthermore, negative interactions in raphe nuclei (dorsal and median) and the BNST implicate pathways along the hypothalamic-pituitary-adrenal (HPA) axis involved in stress response and mood regulation (Somerville et al., 2010). These results support our previous findings that repeated exposure to mild blast results in increased anxiety- and depression-related behaviors in rats (Agoston and Kamnaksh, 2015; Kamnaksh et al., 2011; Kamnaksh et al., 2012; Kovesdi et al., 2012; Kwon et al., 2011).

Neurobehavioral changes coincided with distinct cellular and molecular findings in functionally-relevant brain regions, such as the prefrontal cortex, hippocampus, and amygdala (Kamnaksh et al., 2011; Kamnaksh et al., 2012; Kovesdi et al., 2012; Kwon et al., 2011). The amygdala is anatomically connected to the hippocampus, prefrontal cortex, and hypothalamus, and plays a major role in emotional learning and memory modulation (Bannerman et al., 2004; Kilpatrick and Cahill, 2003). In our current study, the volume of the amygdala increased faster in injured rats. In fact, both the hippocampus and amygdala showed positive injury x age interactions. Altogether these

structures play a central role in the neurobiology of mood disorders (Pêgo et al., 2008).

Matthews et al. previously found increased amygdala activation to fear in veterans with major depressive disorder as a long-term consequence of mbTBI (Matthews et al., 2011a, 2011b). Volumetric increases measured in the amygdala, among other regions, may be related to astroglial hypertrophy that is indicative of neuroinflammation or neurodegeneration in the subacute to chronic phase of the injury. Hypertrophy can also be the result of an increase in dendritic morphology that is correlated with a PTSD-like phenotype associated with neuronal proliferation in the amygdala (Zuckerman et al., 2017). Conversely, injury-induced volumetric decreases can be due to a decline in dendritic arborization at affected regions, changes in fiber caliber (reduced density and/or diameter, depleted neurofilament profiles), as well as neuronal and glial cell damage or loss (Harris et al., 2016; Long et al., 2009).

We previously measured significantly increased levels of neuronal and glial protein biomarkers in peripheral blood up to 70 days post-injury (Ahmed et al., 2013; Kamnaksh et al., 2014; Kwon et al., 2011), including myelin basic protein, neurofilament-heavy chain, neuron-specific enolase, glial fibrillary acidic protein, and tau protein. These biomarkers reflect various ongoing pathologies (e.g., axonal damage, demyelination) in the central nervous system (CNS)—many of which have been associated with neurodegenerative changes in diseases such as chronic traumatic encephalopathy (CTE). Among the most common pathological findings in CTE are cerebral atrophy, thinning of the corpus callosum, neuronal loss, gliosis, and tau-immunoreactive neurofibrillary tangles (McKee et al., 2009, 2016). Therefore, our observed changes in injured rats, supported by significant injury x age interactions on volume, are consistent with progressive neurological deterioration following repetitive brain trauma.

4.2. Diffusion parameters differentially captured the effects of age and injury effects

DTI parameters continued to evolve between the ages of 2 and 5 months, modeling the normal development of human brains (young adult to adult). FA, a normalized measure of microstructural integrity, was the most sensitive at detecting age effects in our current study. Both myelination and synaptogenesis, as well as increasing axonal integrity and connections increase FA (Kochunov et al., 2012), which was higher in older control rats. The other DTI parameters were not as sensitive at detecting voxel-wise age-related changes after multiple comparison correction. However, in uncorrected voxel-wise analyses, radial anisotropy decreased with age in all white matter regions of interest. The decrease in RD in older control animals is related to the same developmental changes that influence the caliber, orientation, and organization of white matter tracts, thereby reducing orthogonal diffusion (Mengler et al., 2014; Niogi and Mukherjee, 2010).

Diffusion metrics were generally better at detecting injury-induced changes in microstructural integrity than age-related changes (Giorgio et al., 2010). We found that DTI parameters were differentially sensitive to short- vs. long-term changes after injury. E1, RD, and ADC increases were extensive at 7 days post-injury, while FA increases in gray and white matter were mostly prominent at 90 days post-injury. Interestingly, these significant (late) FA increases in white matter—involving the cerebral peduncles, cerebellar peduncles and white matter—were not predicted by similar (early) FA increases in all regions. A clinical study of white matter microstructure following traumatic axonal injury found that acute FA was not changed because early increases in E1 and RD values were proportional (Perez et al., 2014). This explains why corrected statistics showed no significant group differences in FA at 7 days post-injury. On the contrary, our uncorrected statistics showed reductions in FA at 7 days post-injury in areas of the corpus callosum, cerebral peduncles, and optic tracts, as well as increases in white matter of the internal capsule and hindbrain. In addition to these white matter regions, E1, RD, and ADC captured injury effects in more frontal white matter tracts, including the anterior commissure, fimbria, and stria medularis.

Relating the above changes in DTI parameters to pathology warrants further study using multiple outcome measures. Pathologic white matter changes, such as demyelination, axonopathy, and partial loss of oligodendroglial cells, can lead to reductions in FA and increases in RD and E1. Conversely, axonal sprouting/regeneration, remyelination, and reorganization can increase FA and reduce RD and E1. While axial and radial diffusivities have been previously linked to specific white matter pathologies (Budde et al., 2007), interpreting FA indices in white vs. gray matter structures is more challenging. The most widely reported changes, both clinical and experimental, are of reduced FA following TBI (Bendlin et al., 2008; Calabrese et al., 2014; Harris et al., 2016; Yeh et al., 2017); however, FA increases have also been reported (Bazarian et al., 2007; Budde et al., 2011; Li et al., 2017; Rubovitch et al., 2011). Therefore, in the absence of additional outcome measures and longitudinal evidence, the temporal pattern of microstructural changes described in our study reflects a dynamic rmbTBI pathology that involves disorganization in the early phase followed by reorganization in select structures.

4.3. Brain regions show selective vulnerability to repeated mild blast exposure

Human studies provide evidence for an evolving pathology in concussive blast TBI, with long-term changes predominantly affecting the right external capsule, posterior limb of internal capsule, and middle frontal gyrus (Mac Donald et al., 2017a), as well as a progressive decline in functional outcome measures (Mac Donald et al., 2017b). DTI studies examining veterans with a history of mbTBI found multifocal white matter changes in many of the same regions identified in our study, including the corpus callosum, cingulum bundle, and cerebellum (Mac Donald et al., 2011; Jorge et al., 2012; Petrie et al., 2014; Meabon et al., 2016; Yeh et al., 2017). Importantly, structural changes identified by DTI were associated with reduced cerebral glucose metabolism, measured by FDG-PET in the same study (Petrie et al., 2014), and the number of blast exposures correlated with cerebellar FDG uptake (Meabon et al., 2016), highlighting the differential vulnerability of brain regions to blast effects.

Frontal lobe white matter is not only larger and more vulnerable to TBI in humans, it is also associated with changes in other subcortical brain regions (Prins and Giza, 2012). Using DTI tract-specific analyses, Yeh et al. found prominent white matter microstructural injury in chronic mbTBI patients in the front-limbic projection fibers (cingulum bundle, uncinate fasciculus), the fronto-parieto-temporal association fibers (superior longitudinal fasciculus), and the fronto-striatal pathways (anterior thalamic radiation) (Yeh et al., 2017). Importantly, post-concussive and post-traumatic stress disorder (PTSD) symptoms, as well as neuropsychological dysfunction were associated with low FA in the major nodes of compromised neurocircuitry (Yeh et al., 2017). Accordingly, the extent of white matter pathology has been found to be predictive of cognitive deficits (Kraus et al., 2007). The dynamic, non-linear developmental trajectory of white matter tracts supporting cognitive function further underlines the importance of our findings and the potential long-term consequences for young soldiers exposed to repetitive mild blast (Groeschel et al., 2010).

The functional relevance of microstructural changes in the frontal lobe and related neurocircuitry, is beyond the scope of this discussion due to the extensive and fundamental nature of these connections. However, the prevalence of cognitive and affective changes as well as autonomic disruptions among individuals with a history of repeated blast exposure implicates these regions in the long-term sequelae of rmbTBI (Petrie et al., 2014). Similar to the frontal lobe, the anatomical location of the hindbrain plays a major role in its vulnerability to mTBIs. In our study, the most consistent changes in DTI parameters

were found in the hindbrain, most often involving the cerebellum and cerebellar peduncles. Our findings support the observations of Meabon et al. showing that the cerebellum, comprised of a large number of gray-white matter boundaries due to its conserved gyrencephalic structure across species including rodents, is especially vulnerable to repetitive mild injury in both veterans and a mouse model of rmbTBI (Meabon et al., 2016). These findings indicate that blast waves specifically affect brain regions with distinct tissue densities/acoustic impedance like gray-white matter boundaries (Nakagawa et al., 2011).

In summary, focal injury to white matter tracts was detected in the corpus callosum, cerebral and cerebellar peduncles, and the cerebellum. Injury-related microstructural changes were characterized differently by DTI parameters. Injury x age interaction effects on FA, E1, and RD were only detected in uncorrected statistical maps. FA was sensitive to white and gray matter injury, showing a positive interaction effect in both. RD appeared sensitive mostly to changes in white matter properties, showing a negative interaction effect, while E1 was less sensitive at capturing injury × age interaction effects on white matter tracts relative to FA and RD. Importantly, the spatial distribution of injury-related changes identified in our study is consistent with neuroimaging findings in blast-exposed veterans (Mac Donald et al., 2011; Matthews et al., 2011b; Jorge et al., 2012; Hetherington et al., 2014; Petrie et al., 2014; Yeh et al., 2017), signifying the preferential vulnerability of select brain regions to repeated mild blast exposure. In the context of protracted white matter development in males, our findings implicate neurodevelopmental age (at the time of injury) as a major determinant of long-term functional outcome.

4.4. Clinical and technical considerations

Using the rat model of rmbTBI allows us to circumvent important impediments to studying TBI directly in humans, even though DTI is readily available in a clinical setting. These obstacles include factors related to the physical environment of blast (e.g., magnitude, orientation, blast overpressure vs. subconcussive exposure) (Cernak and Noble-Haeusslein, 2010), assessment time relative to injury, protocol standardization, resolution, and so forth (Agoston and Kamnaksh, 2015). Animal models provide controlled environments (Palmer et al., 1993) to study pathophysiology and symptomatology, and to evaluate therapies. While we are cautious about extrapolating findings from rodents to humans for obvious reasons, high-fidelity animal modeling of blast-induced TBI and/or other diseases has tremendous translational value.

Animal models also present challenges for MR imaging and analysis due to the substantially smaller brain size: ~1800 mm^3 in rats vs. ~1300 cm^3 in humans. To address the specific challenges of small animal brain voxel-wise analyses we chose to use ANTs, a top performing software for registration with demonstrated value for both human (Avants et al., 2011) and small animal imaging studies (Badea et al., 2012). We adopted a minimum deformation template (MDT) strategy (Avants et al., 2010), rather than one-to-one registration mapping from each subject to an atlas. While the MDT strategy is more time consuming, it has been shown to increase registration accuracy (Avants et al., 2010) since subjects are only a small deformation away from the template. Because the minimum deformation template is closest to all brains in the study, in terms of shape and intensity, the amount of deformation needed to compensate for in any pairwise registration is reduced, and so is the likelihood and magnitude of errors. Moreover, the topological idiosyncrasies in an individual's anatomy are averaged out by the optimal appearance strategy. The results of a good registration were evident in: 1) the evaluation of template appearance, characterized by high signal-to-noise ratio and sharp white/gray matter boundaries; and 2) the quality of the resulting regional labels, which were visualized as overlays on the fractional anisotropy images. Our approach of smoothing the data before voxel-based analysis may be limited in that it restricts us to observing effects at an a priori defined spatial scale, while possibly ignoring small but relevant clusters (e.g., covering white matter areas). However, smoothing was chosen because it improves normality in a parametric analysis, increases image signal-to-noise ratio, and helps alleviate concerns due to imperfect registration.

A major limitation of our work is the absence of female rats in the study groups. With an increasing number of females in sports and in the military, it is critical to assess sex differences as they relate to injury and age. Although our findings are in rats, and they do not demonstrate the same morphometric sex differences or gross anatomical features (e.g., lissencephalic vs. gyrencephalic cerebral cortex) as higher species, the functional and behavioral implications of repeated mild TBI can be far more severe in humans and vary between the sexes. For instance, the central subdivision of the stria terminalis (BSTc) is (on average) twice as large in men as it is in women, and contains twice the number of somatostatin neurons (Swaab, 2007). Because of the role of the BNST in the HPA axis, males may be at higher risk for developing neuropsychiatric symptoms following injury. Additionally, ratios of total corpus callosum, genu, posterior mid-body, and splenium, relative to the whole brain are significantly higher in females compared to males (Tanaka-Arakawa et al., 2015). Therefore, trauma to the corpus callosum in females may result in more severe interhemispheric disconnection symptoms. Finally, our current rmbTBI model was designed to mimic field scenarios. Sham rats are exposed to the same stressors (i.e., transportation, blast sounds, and anesthesia) as injured rats, because stress is an important co-factor in mbTBI (Kamnaksh et al., 2011; Kwon et al., 2011). Since stress alone can affect dendritic branching and spine density, the effects of the injury described in our study could be far more significant relative to a completely naïve brain.

5. Conclusion

Our multiparameteric DTI study showed that repeated exposure to mild blast overpressure causes transient, as well as persistent microstructural changes in white and gray matter structures. Prominent white matter changes were found in the corpus callosum, fimbria, internal capsule, cerebellar peduncles, and cerebellum. In gray matter, the striatum and thalamus showed significant atrophy, while microstructural changes in the sensory, motor, visual, and cingulate cortex were among the most frequent findings. Although many of the detected changes were subtle, they demostrate the selective vulnerability of brain structures to blast overpressure and the dynamic nature of rmbTBI pathology.

Our study suggests that rmbTBI can alter the course of normal late-phase neurodevelopment, such that injury and age may interact to alleviate injury severity and promote recovery/reorganization in select structures but not others. While injury-induced changes in E1, RD, and ADC had largely subsided by 90 days, and age differences and interactions were only detected in uncorrected statistics and ROI analyses, changes in volume and FA persisted and were detected up to 90 days after injury. Therefore, a higher power future study may be more revealing of the dynamics of ongoing rmbTBI pathomechanisms. This would be critical for differentiating between normal age-associated declines in volume and microstructural integrity, and the role of blast exposure in potentiating neurodegenerative effects or deflecting the neurodevelopmental trajectory of young adults to become more hard-wired for stress.

Importantly, our findings are consistent with clinical reports on the long-term structural and functional effects of blast concussive TBI (Mac Donald et al., 2017a, 2017b). These studies, along with ours, demonstrate that the long-term effects of repetitive mild blast exposure may not be countered in totality by the neuroplasticity of a younger brain. The combined findings advocate for additional experimental work aimed at delineating the molecular underpinnings of these long-term (if not permanent) changes, as well as developing new approaches to mitigate and/or treat the long-term consequences of blast-induced TBI.

Disclosure

The views, opinions, and/or findings contained herein are those of the authors and should not be construed as an official position, policy, or decision of the Department of the Army or the Department of Defense.

Animal handling and treatments were conducted in compliance with the Animal Welfare Act and other Federal statutes and regulations related to animals and experiments involving animals, and adhered to principles stated in the Guide to the Care and Use of Laboratory Animals, National Research Council. The facilities are fully accredited by the Association for Assessment and Accreditation of Laboratory Animal Care International.

The authors declare no competing financial interests.

Supplementary data to this article can be found online at https://doi.org/10.1016/j.nicl.2018.01.007.

Acknowledgements

We thank the Neurotrauma Team at the Walter Reed Army Institute of Research (WRAIR) for their technical help during the exposures. We also thank Dr. G. Allan Johnson for critically reading the manuscript. This work was supported by the United States Army Medical Research Acquisition Activity (USAMRAA) grant number G1702174, and WRAIR grant number G170353315. Imaging was done at the Center for In Vivo Microscopy, supported through NIH/NIBIB awards P41 EB015897 and 1S10OD010683-01. AB gratefully acknowledges support from NIH/NIA through K01 AG041211.

References

Acosta, S.A., Tajiri, N., de la Pena, I., Bastawrous, M., Sanberg, P.R., Kaneko, Y., Borlongan, C.V., 2015. Alpha-synuclein as a pathological link between chronic traumatic brain injury and Parkinson's disease. J. Cell. Physiol. 230, 1024–1032.

Agoston, D., Kamnaksh, A., 2015. In: Firas (Ed.), Modeling the Neurobehavioral Consequences of Blast-Induced Traumatic Brain Injury Spectrum Disorder and Identifying Related Biomarkers.

Ahmed, F.A., Kamnaksh, A., Kovesdi, E., Long, J.B., Agoston, D.V., 2013. Long-term consequences of single and multiple mild blast exposure on select physiological parameters and blood-based biomarkers. Electrophoresis 34, 2229–2233.

Asato, M.R., Terwilliger, R., Woo, J., Luna, B., 2010. White matter development in adolescence: a DTI study. Cereb. Cortex 20, 2122–2131.

Avants, B.B., Yushkevich, P., Pluta, J., Minkoff, D., Korczykowski, M., Detre, M., Gee, J.C., 2010. The optimal template effect in hippocampus studies of diseased populations. NeuroImage 49, 2457–2466.

Avants, B.B., Tustison, N.J., Song, G., Cook, P.A., Klein, A., Gee, J.C., 2011. A reproducible evaluation of ANTs similarity metric performance in brain image registration. NeuroImage 54, 2033–2044.

Badea, A., Ali-Sharief, A.A., Johnson, G.A., 2007. Morphometric analysis of the C57BL/6J mouse brain. NeuroImage 37, 683–693.

Badea, A., Gewalt, S., Avants, B.B., Cook, J.J., Johnson, G.A., 2012. Quantitative mouse brain phenotyping based on single and multispectral MR protocols. NeuroImage 63, 1633–1645.

Bannerman, D.M., Rawlins, J.N., McHugh, S.B., Deacon, R.M., Yee, B.K., Bast, T., Zhang, W.N., Pothuizen, H.H., Feldon, J., 2004. Regional dissociations within the hippocampus—memory and anxiety. Neurosci. Biobehav. Rev. 28, 273–283.

Bauman, R.A., Ling, G., Tong, L., Januszkiewicz, A., Agoston, D., Delanerolle, N., Kim, Y., Ritzel, D., Bell, R., Ecklund, J., Armonda, R., Bandak, F., Parks, S., 2009. An introductory characterization of a combat-casualty-care relevant swine model of closed head injury resulting from exposure to explosive blast. J. Neurotrauma 26, 841–860.

Bazarian, J.J., Zhong, J., Blyth, B., Zhu, T., Kavcic, V., Peterson, D., 2007. Diffusion tensor imaging detects clinically important axonal damage after mild traumatic brain injury: a pilot study. J. Neurotrauma 24, 1447–1459.

Belanger, H.G., Vanderploeg, R.D., Curtiss, G., Warden, D.L., 2007. Recent neuroimaging techniques in mild traumatic brain injury. J. Neuropsychiatr. Clin. Neurosci. 19, 5–20.

Bendlin, B.B., Ries, M.L., Lazar, M., Alexander, A.L., Dempsey, R.J., Rowley, H.A., Sherman, J.E., Johnson, S.C., 2008. Longitudinal changes in patients with traumatic brain injury assessed with diffusion-tensor and volumetric imaging. NeuroImage 42, 503–514.

Budde, M.D., Kim, J.H., Liang, H.F., Schmidt, R.E., Russell, J.H., Cross, A.H., Song, S.K., 2007. Toward accurate diagnosis of white matter pathology using diffusion tensor imaging. Magn. Reson. Med. 57, 688–695.

Budde, M.D., Janes, L., Gold, E., Turtzo, L.C., Frank, J.A., 2011. The contribution of gliosis to diffusion tensor anisotropy and tractography following traumatic brain injury: validation in the rat using Fourier analysis of stained tissue sections. Brain 134, 2248–2260.

Calabrese, E., Badea, A., Watson, C., Johnson, G.A., 2013. A quantitative magnetic resonance histology atlas of postnatal rat brain development with regional estimates of growth and variability. NeuroImage 71, 196–206.

Calabrese, E., Du, F., Garman, R.H., Johnson, G.A., Riccio, C., Tong, L.C., Long, J.B., 2014. Diffusion tensor imaging reveals white matter injury in a rat model of repetitive blast-induced traumatic brain injury. J. Neurotrauma 31, 938–950.

Cernak, I., Noble-Haeusslein, L.J., 2010. Traumatic brain injury: an overview of pathobiology with emphasis on military populations. J. Cereb. Blood Flow Metab. 30, 255–266.

Daneshvar, D.H., Goldstein, L.E., Kiernan, P.T., Stein, T.D., McKee, A.C., 2015. Post-traumatic neurodegeneration and chronic traumatic encephalopathy. Mol. Cell. Neurosci. 66, 81–90.

Emery, D.L., Royo, N.C., Fischer, I., Saatman, K.E., McIntosh, T.K., 2003. Plasticity following injury to the adult central nervous system: is recapitulation of a developmental state worth promoting? J. Neurotrauma 20, 1271–1292.

Friston, K.J., Holmes, A.P., Worsley, K.J., Poline, J.P., Frith, C.D., Frackowiak, R.S.J., 1994. Statistical parametric maps in functional imaging: a general linear approach. Hum. Brain Mapp. 2, 189–210.

Friston, K.J., Penny, W.D., Ashburner, J., Kiebel, S.J., Nichols, T.E., 2006. Statistical Parametric Mapping : The Analysis of Functional Brain Images. Academic Press, London.

Gardner, R.C., Yaffe, K., 2015. Epidemiology of mild traumatic brain injury and neurodegenerative disease. Mol. Cell. Neurosci. 66 (Part B), 75–80.

Gavett, B.E., Stern, R.A., McKee, A.C., 2011. Chronic traumatic encephalopathy: a potential late effect of sport-related concussive and subconcussive head trauma. Clin. Sports Med. 30, 179–188 (xi).

Giorgio, A., Santelli, L., Tomassini, V., Bosnell, R., Smith, S., De Stefano, N., Johansen-Berg, H., 2010. Age-related changes in grey and white matter structure throughout adulthood. NeuroImage 51, 943–951.

Goldstein, M., 1990. Traumatic brain injury: a silent epidemic. Ann. Neurol. 27, 327.

Gritti, A., Vescovi, A.L., Galli, R., 2002. Adult neural stem cells: plasticity and developmental potential. J. Physiol. Paris 96, 81–90.

Groeschel, S., Vollmer, B., King, M.D., Connelly, A., 2010. Developmental changes in cerebral grey and white matter volume from infancy to adulthood. Int. J. Dev. Neurosci. 28, 481–489.

Harris, N.G., Verley, D.R., Gutman, B.A., Sutton, R.L., 2016. Bi-directional changes in fractional anisotropy after experiment TBI: disorganization and reorganization? NeuroImage 133, 129–143.

Hetherington, H.P., Hamid, H., Kulas, J., Ling, G., Bandak, F., de Lanerolle, N.C., Pan, J.W., 2014. MRSI of the medial temporal lobe at 7 T in explosive blast mild traumatic brain injury. Magn. Reson. Med. 71, 1358–1367.

Huang, D., Xu, J., Wang, J., Tong, J., Bai, X., Li, H., Wang, Z., Huang, Y., Wu, Y., Yu, M., Huang, F., 2017. Dynamic changes in the nigrostriatal pathway in the MPTP mouse model of Parkinson's disease. Parkinsons Dis. 2017, 9349487.

Institute of, M, 2013. Returning Home from Iraq and Afghanistan: Assessment of Readjustment Needs of Veterans, Service Members, and Their Families. The National Academies Press, Washington, DC.

Iverson, G.L., Gardner, A.J., McCrory, P., Zafonte, R., Castellani, R.J., 2015. A critical review of chronic traumatic encephalopathy. Neurosci. Biobehav. Rev. 56, 276–293.

Jagoda, A.S., Bazarian, J.J., Bruns Jr., J.J., Cantrill, S.V., Gean, A.D., Howard, P.K., Ghajar, J., Riggio, S., Wright, D.W., Wears, R.L., Bakshy, A., Burgess, P., Wald, M.M., Whitson, R.R., 2008. Clinical policy: neuroimaging and decisionmaking in adult mild traumatic brain injury in the acute setting. Ann. Emerg. Med. 52, 714–748.

Johnson, G.A., Calabrese, E., Badea, A., Paxinos, G., Watson, C., 2012. A multidimensional magnetic resonance histology atlas of the Wistar rat brain. NeuroImage 62, 1848–1856.

Johnson, V.E., Stewart, J.E., Begbie, F.D., Trojanowski, J.Q., Smith, D.H., Stewart, W., 2013. Inflammation and white matter degeneration persist for years after a single traumatic brain injury. Brain 136, 28–42.

Jorge, R.E., Acion, L., White, T., Tordesillas-Gutierrez, D., Pierson, R., Crespo-Facorro, B., Magnotta, V.A., 2012. White matter abnormalities in veterans with mild traumatic brain injury. Am. J. Psychiatry 169, 1284–1291.

Kamnaksh, A., Kovesdi, E., Kwon, S.K., Wingo, D., Ahmed, F., Grunberg, N.E., Long, J., Agoston, D.V., 2011. Factors affecting blast traumatic brain injury. J. Neurotrauma 28, 2145–2153.

Kamnaksh, A., Kwon, S.K., Kovesdi, E., Ahmed, F., Barry, E.S., Grunberg, N.E., Long, J., Agoston, D., 2012. Neurobehavioral, cellular, and molecular consequences of single and multiple mild blast exposure. Electrophoresis 33, 3680–3692.

Kovesdi, E., E.B., N.G., J.L., Agoston, D., 2014. Molecular mechanisms of increased vulnerability after repeated mild blast-induced traumatic brain injury. Transl. Proteom. 3, 22–37.

Kilpatrick, L., Cahill, L., 2003. Amygdala modulation of parahippocampal and frontal regions during emotionally influenced memory storage. NeuroImage 20, 2091–2099.

Kochunov, P., Williamson, D.E., Lancaster, J., Fox, P., Cornell, J., Blangero, J., Glahn, D.C., 2012. Fractional anisotropy of water diffusion in cerebral white matter across the lifespan. Neurobiol. Aging 33, 9–20.

Kolb, B., Cioe, J., Muirhead, D., 1998. Cerebral morphology and functional sparing after prenatal frontal cortex lesions in rats. Behav. Brain Res. 91, 143–155.

Kovesdi, E., Gyorgy, A.B., Kwon, S.K., Wingo, D.L., Kamnaksh, A., Long, J.B., Kasper, C.E., Agoston, D.V., 2012. The effect of enriched environment on the outcome of traumatic brain injury; a behavioral, proteomics, and histological study. Front. Neurosci. 5, 42.

Kraus, M.F., Susmaras, T., Caughlin, B.P., Walker, C.J., Sweeney, J.A., Little, D.M., 2007. White matter integrity and cognition in chronic traumatic brain injury: a diffusion tensor imaging study. Brain 130, 2508–2519.

Kwon, S.K., Kovesdi, E., Gyorgy, A.B., Wingo, D., Kamnaksh, A., Walker, J., Long, J.B.,

Agoston, D.V., 2011. Stress and traumatic brain injury: a behavioral, proteomics, and histological study. Front. Neurol. 2 (12).
Leow, A., Chiang, M.-C., Huang, S.C., Toga, A.W., Thompson, P.M., 2006. Realizing Unbiased Deformation: A Theoretical Consideration. 1st MICCAI Workshop on Mathematical Foundations of Computational Anatomy: Geometrical, Statistical and Registration Methods for Modeling Biological Shape Variability, Copenhagen, Denmark. pp. 174–181.
Lewis, M.H., 2004. Environmental complexity and central nervous system development and function. Ment. Retard. Dev. Disabil. Res. Rev. 10, 91–95.
Li, J., Zhao, C., Rao, J.S., Yang, F.X., Wang, Z.J., Lei, J.F., Yang, Z.Y., Li, X.G., 2017. Structural and metabolic changes in the traumatically injured rat brain: high-resolution in vivo proton magnetic resonance spectroscopy at 7 T. Neuroradiology 59, 1203–1212.
Ling, G.S., Ecklund, J.M., 2011. Traumatic brain injury in modern war. Curr. Opin. Anaesthesiol. 24, 124–130.
Ling, J.M., Peña, A., Yeo, R.A., Merideth, F.L., Klimaj, S., Gasparovic, C., Mayer, A.R., 2012. Biomarkers of increased diffusion anisotropy in semi-acute mild traumatic brain injury: a longitudinal perspective. Brain 135, 1281–1292.
Long, J.B., Bentley, T.L., Wessner, K.A., Cerone, C., Sweeney, S., Bauman, R.A., 2009. Blast overpressure in rats: recreating a battlefield injury in the laboratory. J. Neurotrauma. 26 (6), 827–840.
Mac Donald, C.L., Johnson, A.M., Cooper, D., Nelson, E.C., Werner, N.J., Shimony, J.S., Snyder, A.Z., Raichle, M.E., Witherow, J.R., Fang, R., Flaherty, S.F., Brody, D.L., 2011. Detection of blast-related traumatic brain injury in U.S. military personnel. N. Engl. J. Med. 364, 2091–2100.
Mac Donald, C., Johnson, A., Cooper, D., Malone, T., Sorrell, J., Shimony, J., Parsons, M., Snyder, A., Raichle, M., Fang, R., Flaherty, S., Russell, M., Brody, D.L., 2013. Cerebellar white matter abnormalities following primary blast injury in US military personnel. PLoS One 8, e55823.
Mac Donald, C.L., Barber, J., Andre, J., Evans, N., Panks, C., Sun, S., Zalewski, K., Elizabeth Sanders, R., Temkin, N., 2017a. 5-Year imaging sequelae of concussive blast injury and relation to early clinical outcome. Neuroimage Clin. 14, 371–378.
Mac Donald, C.L., Barber, J., Jordan, M., Johnson, A.M., Dikmen, S., Fann, J.R., Temkin, N., 2017b. Early clinical predictors of 5-year outcome after concussive blast traumatic brain injury. JAMA Neurol. 74 (7), 821–829.
MacFarlane, M.P., Glenn, T.C., 2015. Neurochemical cascade of concussion. Brain Inj. 29, 139–153.
Matsushita, M., Hosoda, K., Naitoh, Y., Yamashita, H., Kohmura, E., 2011. Utility of diffusion tensor imaging in the acute stage of mild to moderate traumatic brain injury for detecting white matter lesions and predicting long-term cognitive function in adults. J. Neurosurg. 115, 130–139.
Matthews, S., Simmons, A., Strigo, I., 2011a. The effects of loss versus alteration of consciousness on inhibition-related brain activity among individuals with a history of blast-related concussion. Psychiatry Res. 191, 76–79.
Matthews, S.C., Strigo, I.A., Simmons, A.N., O'Connell, R.M., Reinhardt, L.E., Moseley, S.A., 2011b. A multimodal imaging study in U.S. veterans of Operations Iraqi and Enduring Freedom with and without major depression after blast-related concussion. NeuroImage 54 (Suppl. 1), S69–75.
McKee, A.C., Cantu, R.C., Nowinski, C.J., Hedley-Whyte, E.T., Gavett, B.E., Budson, A.E., Santini, V.E., Lee, H.S., Kubilus, C.A., Stern, R.A., 2009. Chronic traumatic encephalopathy in athletes: progressive tauopathy after repetitive head injury. J. Neuropathol. Exp. Neurol. 68, 709–735.
McKee, A.C., Stein, T.D., Kiernan, P.T., Alvarez, V.E., 2015. The neuropathology of chronic traumatic encephalopathy. Brain Pathol. 25, 350–364.
McKee, A.C., Cairns, N.J., Dickson, D.W., Folkerth, R.D., Dirk Keene, C., Litvan, I., Perl, D.P., Stein, T.D., Vonsattel, J.P., Stewart, W., Tripodis, Y., Crary, J.F., Bieniek, K.F., Dams-O'Connor, K., Alvarez, V.E., Gordon, W.A., 2016. The first NINDS/NIBIB consensus meeting to define neuropathological criteria for the diagnosis of chronic traumatic encephalopathy. Acta Neuropathol. 131, 75–86.
Meabon, J.S., Huber, B.R., Cross, D.J., Richards, T.L., Minoshima, S., Pagulayan, K.F., Li, G., Meeker, K.D., Kraemer, B.C., Petrie, E.C., Raskind, M.A., Peskind, E.R., Cook, D.G., 2016. Repetitive blast exposure in mice and combat veterans causes persistent cerebellar dysfunction. Sci. Transl. Med. 8, 321ra326.
Mengler, L., Khmelinskii, A., Diedenhofen, M., Po, C., Staring, M., Lelieveldt, B.P., Hoehn, M., 2014. Brain maturation of the adolescent rat cortex and striatum: changes in volume and myelination. NeuroImage 84, 35–44.
Nakagawa, A., Manley, G.T., Gean, A.D., Ohtani, K., Armonda, R., Tsukamoto, A., Yamamoto, H., Takayama, K., Tominaga, T., 2011. Mechanisms of primary blast-induced traumatic brain injury: insights from shock-wave research. J. Neurotrauma 28, 1101–1119.
Niogi, S.N., Mukherjee, P., 2010. Diffusion tensor imaging of mild traumatic brain injury. J. Head Trauma Rehabil. 25, 241–255.
Palmer, A.M., Marion, D.W., Botscheller, M.L., Swedlow, P.E., Styren, S.D., DeKosky, S.T., 1993. Traumatic brain injury-induced excitotoxicity assessed in a controlled cortical impact model. J. Neurochem. 61, 2015–2024.
Pêgo, J.M., Morgado, P., Pinto, L.G., Cerqueira, J.J., Almeida, O.F.X., Sousa, N., 2008. Dissociation of the morphological correlates of stress-induced anxiety and fear. Eur. J. Neurosci. 27, 1503–1516.
Perez, A.M., Adler, J., Kulkarni, N., Strain, J.F., Womack, K.B., Diaz-Arrastia, R., Marquez de la Plata, C.D., 2014. Longitudinal white matter changes after traumatic axonal injury. J. Neurotrauma 31, 1478–1485.
Petrie, E.C., Cross, D.J., Yarnykh, V.L., Richards, T., Martin, N.M., Pagulayan, K., Hoff, D., Hart, K., Mayer, C., Tarabochia, M., Raskind, M.A., Minoshima, S., Peskind, E.R., 2014. Neuroimaging, behavioral, and psychological sequelae of repetitive combined blast/impact mild traumatic brain injury in Iraq and Afghanistan war veterans. J. Neurotrauma 31, 425–436.
Prins, M.L., Giza, C.C., 2012. Repeat traumatic brain injury in the developing brain. Int. J. Dev. Neurosci. 30, 185–190.
Rubovitch, V., Ten-Bosch, M., Zohar, O., Harrison, C.R., Tempel-Brami, C., Stein, E., Hoffer, B.J., Balaban, C.D., Schreiber, S., Chiu, W.T., Pick, C.G., 2011. A mouse model of blast-induced mild traumatic brain injury. Exp. Neurol. 232, 280–289.
Scahill, R.I., Frost, C., Jenkins, R., Whitwell, J.L., Rossor, M.N., Fox, N.C., 2003. A longitudinal study of brain volume changes in normal aging using serial registered magnetic resonance imaging. Arch. Neurol. 60, 989–994.
Selemon, L.D., 2013. A role for synaptic plasticity in the adolescent development of executive function. Transl. Psychiatry 3, e238.
Semple, B.D., Blomgren, K., Gimlin, K., Ferriero, D.M., Noble-Haeusslein, L.J., 2013. Brain development in rodents and humans: identifying benchmarks of maturation and vulnerability to injury across species. Prog. Neurobiol. 106-107, 1–16.
Signoretti, S., Lazzarino, G., Tavazzi, B., Vagnozzi, R., 2011. The pathophysiology of concussion. PM R 3, S359–368.
Simmonds, D.J., Hallquist, M.N., Asato, M., Luna, B., 2014. Developmental stages and sex differences of white matter and behavioral development through adolescence: a longitudinal diffusion tensor imaging (DTI) study. NeuroImage 92, 356–368.
Somerville, L.H., Whalen, P.J., Kelley, W.M., 2010. Human bed nucleus of the stria terminalis indexes hypervigilant threat monitoring. Biol. Psychiatry 68, 416–424.
Sowell, E.R., Thompson, P.M., Holmes, C.J., Jernigan, T.L., Toga, A.W., 1999. In vivo evidence for post-adolescent brain maturation in frontal and striatal regions. Nat. Neurosci. 2, 859–861.
Sowell, E.R., Thompson, P.M., Tessner, K.D., Toga, A.W., 2001. Mapping continued brain growth and gray matter density reduction in dorsal frontal cortex: inverse relationships during postadolescent brain maturation. J. Neurosci. 21, 8819–8829.
Sowell, E.R., Trauner, D.A., Gamst, A., Jernigan, T.L., 2002. Development of cortical and subcortical brain structures in childhood and adolescence: a structural MRI study. Dev. Med. Child Neurol. 44, 4–16.
Stejskal, E.O., Tanner, J.E., 1965. Spin diffusion measurements: spin echoes in the presence of a time-dependent field gradient. J. Chem. Phys. 42, 288–292.
Sumiyoshi, A., Nonaka, H., Kawashima, R., 2017. Sexual differentiation of the adolescent rat brain: a longitudinal voxel-based morphometry study. Neurosci. Lett. 642, 168–173.
Swaab, D.F., 2007. Sexual differentiation of the brain and behavior. Best Pract. Res. Clin. Endocrinol. Metab. 21, 431–444.
Tanaka-Arakawa, M.M., Matsui, M., Tanaka, C., Uematsu, A., Uda, S., Miura, K., Sakai, T., Noguchi, K., 2015. Developmental changes in the corpus callosum from infancy to early adulthood: a structural magnetic resonance imaging study. PLoS One 10, e0118760.
Tansey, M.G., McCoy, M.K., Frank-Cannon, T.C., 2007. Neuroinflammatory mechanisms in Parkinson's disease: potential environmental triggers, pathways, and targets for early therapeutic intervention. Exp. Neurol. 208, 1–25.
U.S. Department of Health and Human Services, C.f.D.C.a.P, 2009. Heads Up: Facts for Physicians About Mild Traumatic Brain Injury (MTBI), 2009. http://www.brainlinemilitary.org/concussion_course/course_content/pdfs/mtbi.pdf (Accessed 4/30/2017 (23 pp.)).
Voss, J.D., Connolly, J., Schwab, K.A., Scher, A.I., 2015. Update on the epidemiology of concussion/mild traumatic brain injury. Curr. Pain Headache Rep. 19 (32).
Wang, R., Benner, T., Sorensen, A., Wedeen, V., 2007. Diffusion toolkit: a software package for diffusion imaging data processing and tractography - 03720.pdf. Proc. Int. Soc. Magn. Reson. Med. 15, 3720.
Winston, C.N., Noel, A., Neustadtl, A., Parsadanian, M., Barton, D.J., Chellappa, D., Wilkins, T.E., Alikhani, A.D., Zapple, D.N., Villapol, S., Planel, E., Burns, M.P., 2016. Dendritic spine loss and chronic white matter inflammation in a mouse model of highly repetitive head trauma. Am. J. Pathol. 186, 552–567.
Yeh, P.H., Guan Koay, C., Wang, B., Morissette, J., Sham, E., Senseney, J., Joy, D., Kubli, A., Yeh, C.H., Eskay, V., Liu, W., French, L.M., Oakes, T.R., Riedy, G., Ollinger, J., 2017. Compromised neurocircuitry in chronic blast-related mild traumatic brain injury. Hum. Brain Mapp. 38, 352–369.
Zuckerman, A., Ram, O., Ifergane, G., Matar, M.A., Sagi, R., Ostfeld, I., Hoffman, J.R., Kaplan, Z., Sadot, O., Cohen, H., 2017. Controlled low-pressure blast-wave exposure causes distinct behavioral and morphological responses modelling mild traumatic brain injury, post-traumatic stress disorder, and comorbid mild traumatic brain injury-post-traumatic stress disorder. J. Neurotrauma 34, 145–164.